

## Research Article

# Exploring the potential of *ex-vivo* 7-T magnetic resonance imaging on patients with clinically significant prostate cancer: visibility and size perspective<sup>☆</sup>

Hyungwoo Ahn<sup>a,\*,\*</sup>, Jung Kwon Kim<sup>b,\*</sup>, Sung Il Hwang<sup>a</sup>, Sung Kyu Hong<sup>b</sup>,  
Seok-Soo Byun<sup>b</sup>, Sang Hun Song<sup>b</sup>, Gheeyoung Choe<sup>c</sup>, Hye Mi Jee<sup>d</sup>, Sung Woo Park<sup>e</sup>

<sup>a</sup> Department of Radiology, Seoul National University Bundang Hospital, Seongnam, Korea

<sup>b</sup> Department of Urology, Seoul National University Bundang Hospital, Seongnam, Korea

<sup>c</sup> Department of Pathology, Seoul National University Bundang Hospital, Seongnam, Korea

<sup>d</sup> Preclinical Research Center, Seoul National University Bundang Hospital, Seongnam, Korea

<sup>e</sup> Department of Biomedical Engineering, Seoul National University Hospital, Seoul, Korea

## ARTICLE INFO

## Article history:

Received 17 January 2024

Received in revised form

13 February 2024

Accepted 19 February 2024

Available online 22 February 2024

## Keywords:

Biopsy

Magnetic resonance imaging

Prastatotomy

Prostatic neoplasms

## ABSTRACT

**Background:** Despite progress in multiparametric magnetic resonance imaging (MRI), issues of prostate cancer invisibility and underestimated tumor burden persist. This study investigates the potential of an ultra-high field MRI at 7-T in an *ex-vivo* setting to address these limitations.

**Methods:** This prospective study included 54 tumors from 20 treatment-naïve clinically significant prostate cancer patients, confirmed by biopsy, despite negative findings on preoperative 3-T MRI. *Ex-vivo* 7-T MRI of resected prostates was performed, with assessment on tumor visibility and size. Factors influencing visibility were analyzed using logistic regression analyses.

**Results:** Tumor visibility was confirmed in 80% of patients, and 48% of all tumors on *ex-vivo* imaging. Gleason pattern 4 percentage (odds ratio 1.09) and tumor size on pathology (odds ratio 1.36) were significantly associated with visibility ( $P < 0.05$ ). Mean MRI-visible and invisible tumor sizes were 10.5 mm and 5.3 mm, respectively. The size discrepancy between MRI and pathology was 2.7 mm.

**Conclusion:** Tumor visibility on *ex-vivo* 7-T MRI was influenced by tumor grade and size. The notable tumor visibility initially overlooked on 3-T MRI, along with small size discrepancy with pathology, suggests potential improvements in resolution.

© 2024 The Asian Pacific Prostate Society. Published by Elsevier B.V. This is an open access article under the CC BY-NC-ND license (<http://creativecommons.org/licenses/by-nc-nd/4.0/>).

## 1. Introduction

Prostate cancer (PCa) remains the second most common cancer among men, significantly contributing to overall cancer-related deaths<sup>1</sup>. Traditionally, PCa diagnosis relied on systematic biopsies in patients with elevated prostate-specific antigen (PSA) levels, leading to the dual challenge of overdiagnosing clinically insignificant PCa and underdiagnosing clinically significant (cs) tumors. The advent of multiparametric (mp) magnetic resonance imaging (MRI) and the Prostate Imaging-Reporting and Data System (PIRADS) transformed PCa diagnosis, emphasizing targeted biopsies for potential csPCa based on mpMRI findings<sup>2</sup>.

However, current prostate MRI at 1.5 or 3-Tesla (T) magnetic strength reportedly misses over 10% of csPCa, raising controversy over the complete omission of systematic biopsies<sup>3,4</sup>. This diagnostic challenge is compounded by the consistent shortfall of prostate MRI in accurately assessing the true tumor burden compared to pathological evaluations<sup>5,6</sup>. The resulting underestimation on MRI may pose a risk of guiding treatment decisions misaligned with the actual pathological context.

To address this challenge, achieving superior tumor resolution through imaging is essential, and ultra-high field (UHF) MRI at 7-T or higher may play a role as a promising candidate. Studies have reported excellent signal-to-noise ratios in 7-T prostate MRI, indicating its potential<sup>7,8</sup>. However, UHF prostate MRI in human subjects remains experimental, due to concerns about radiofrequency field inhomogeneity and potential heating effects related to high local specific absorption rate<sup>9</sup>. Conversely, *ex-vivo* MRI of resected prostates avoids safety concerns and exhibits spatial resolution comparable to low-power field microscopy<sup>10</sup>.

<sup>☆</sup> This work was supported by a research grant from Seoul National University Bundang Hospital (14-2019-0032).

\* Corresponding author.

E-mail address: [iahnyungwoo@gmail.com](mailto:iahnyungwoo@gmail.com) (H. Ahn).

<sup>\*</sup> Hyungwoo Ahn and Jung Kwon Kim contributed equally to this work.

Our goal was to investigate whether UHF MRI performed in an *ex-vivo* setting without safety concerns, could effectively address the existing challenges in MRI. In pursuit of this, we explored whether UHF MRI demonstrates superior tumor visualization compared to conventional MRI and analyzed the influencing factors. Additionally, we assessed whether UHF MRI could reduce the size difference when compared to tumors measured pathologically.

## 2. Materials and methods

### 2.1. Study cohort

This prospective study received an approval from the Institutional Review Board before initiation, and informed consent was obtained from all participants. Based upon the assumption that a 7-T MRI would offer superior tumor visibility compared to a 3-T MRI, we included 20 consecutive treatment-naïve patients who were diagnosed with csPCa, defined as tumors of Gleason score (GS)  $\geq 7$  (3 + 4), in spite of absence of any lesion with a PIRADS score  $\geq 4$ . The preoperative MRI scans were taken at 3-T magnetic strength, and were interpreted by board-certified radiologists with 11- and 7-years of experience of PIRADS categorization as a routine daily practice. The participants subsequently underwent radical prostatectomy (RP) within 2 months from the time of preoperative MRI.

### 2.2. Specimen handling

On the day of surgery, the RP specimens were placed into a saline-filled container and transported to our in-house preclinical research facility within 10 minutes. There, the specimen was transferred to another container filled with perfluorohexane (Fluorinert, 3M, MN, USA), to prevent susceptibility artifacts that may arise during an *ex-vivo* MRI acquisition. The container was specially designed to fit onto a 65 mm bored MRI-compatible animal imaging bed. The imaging bed with the container holding the specimens was then subjected to imaging using a preclinical MRI system for small animals (Powerscan 7.0-T, MR Solutions, Surrey, UK) (Fig. 1).

After conducting an *ex-vivo* imaging, the specimen was taken out from the Fluorinert-filled container, rinsed with saline, and transported back to the pathology department. After being fixated in a 10% buffered formalin for 24 hours, the specimen was sliced into 3-millimeter sections perpendicular to the distal urethra.

### 2.3. Assessment of the specimen

The *ex-vivo* specimen MRI taken at 7-T magnetic strength was interpreted by a consensus of the two radiologists who assessed the preoperative MRI. Although radiologists were inevitably aware of

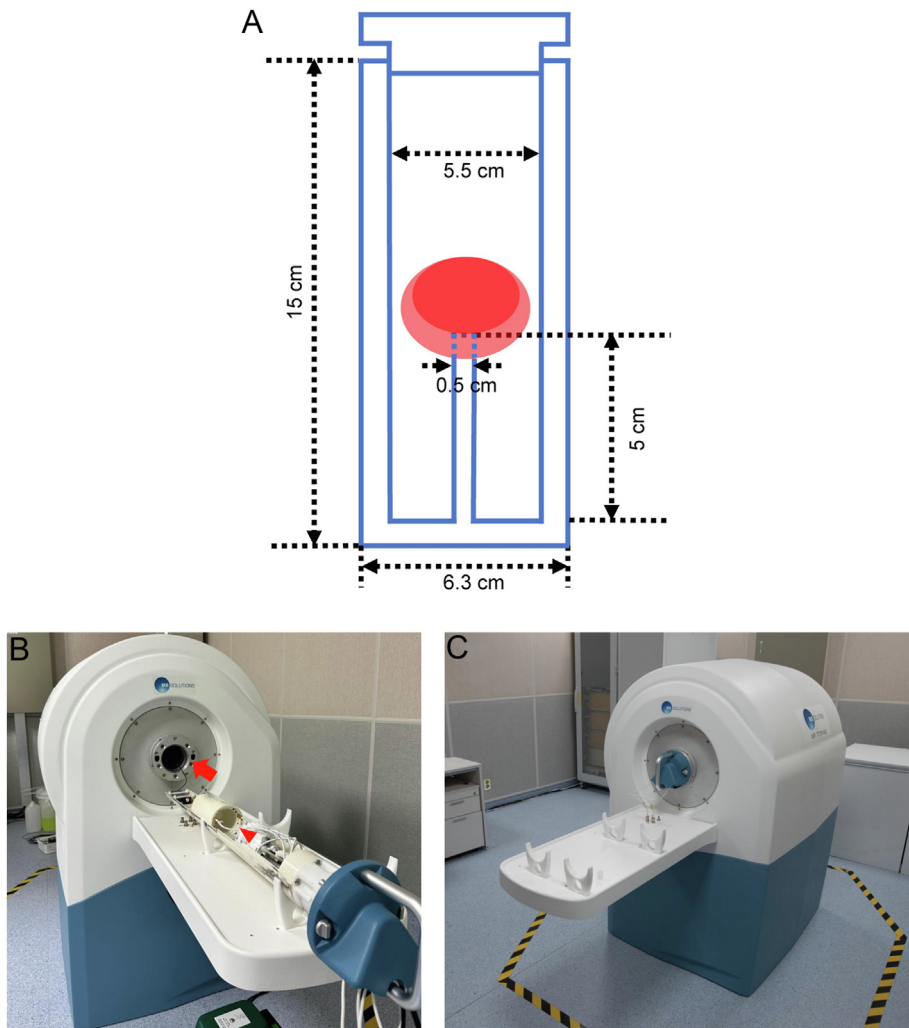


**Fig. 1.** An overview of the specimen imaging. (A) The excised prostate (red ellipse) was carefully positioned within a custom-made perfluorohexane-filled container. The specimen was fixed at the distal urethra, serving as the imaging axis. (B) Subsequently, the container was reintroduced onto an animal imaging bed (arrowhead) and inserted into the scanner (arrow). (C) The prepared specimen was imaged using the preclinical 7-T scanner.

the presence of PCa in the specimen, they evaluated the *ex-vivo* MRI before pathological evaluation was performed. Since imaging was conducted on excised specimens, dynamic contrast-enhanced (DCE) MRI was not feasible. Therefore, biparametric (bp) MRI was performed. The parameters were as follows: for turbo spin echo T2-weighted imaging, slice thickness 3 mm, no gap, repetition time 4000 ms, echo time 114 ms, number of signal averages= 4, matrix size 512 × 512; for spin-echo diffusion weighted imaging, slice thickness of 3 mm, no gap, repetition time 3600 ms, echo time 34 ms, matrix size 256 × 256, b-values of 0 and 1000 s/mm<sup>2</sup>. Axial plane images were acquired perpendicular to the distal prostatic urethra. For suspicious lesions detected on the *ex-vivo* MRI, the radiologists assigned PIRADS score and measured the greatest dimension. Tumor was considered visible when categorized as PIRADS score 4 or 5. For histopathological evaluation, a single-experienced board-certified pathologist examined the specimen, and recorded the number, size, volume, Gleason score (GS), and location of each tumor focus. The Gleason pattern 4 (GP4) percentage in each tumor was also recorded. The index tumor was defined in a similar manner for both radiology and pathology: the lesion assigned of the highest PIRADS score or GS, and the lesion with greatest dimension among the same score group.

The radiologists and the pathologist also used the same sector map to locate the tumors: the lower one-third of the prostate defined as an apex, mid one-third as a midgland, and the upper one-third as a base; a horizontal line crossing the midsection of the prostatic urethra was used as a landmark dividing anterior and posterior gland.

A lesion was considered concordant between radiology and pathology if it is either demonstrating perfect sector-match, or at least one intersecting sector with mismatches within one neighboring sector on MRI and pathology.

#### 2.4. Statistical analysis

The normal distribution of the data was assessed using the Shapiro–Wilk test. For normally distributed data, mean and standard deviation (SD) were presented, while for non-normally distributed data, median and inter-quartile range (IQR) were provided.

The characteristics comparison between patients with confirmed tumor visibility and those without, as well as the comparison between the size of concordant tumors measured on MRI and pathology was carried out using either the student's t-test or Mann–Whitney test, depending upon the normality of the distribution of the data.

A logistic regression analysis was performed, to identify factors associated with the visibility of each lesion. Variables showing significance at the  $P < 0.10$  level in a univariable analysis were included in the multivariable analysis. The reason for choosing a relatively more lenient cut-off was that its purpose was to identify potential predictor variables rather than to test a hypothesis<sup>11</sup>. For significant factors, their performance was verified through receiver-operating characteristics (ROC) analysis.

Statistical analysis was conducted using the R (statistical programming language) version 4.3.2, and a  $P$ -value  $< 0.05$  was considered statistically significant.

#### 2.5. Literature search

The main goal of this study was to evaluate if an *ex-vivo* 7-T MRI enhances the detection of PCa compared to a conventional 3-T MRI. An ideal comparison between 3-T and *ex-vivo* 7-T MRI results could not be conducted as this study focuses solely on patients with an invisible PCa on a 3-T MRI. To overcome this limitation, we

performed a literature search for identified factors influencing tumor visibility in the logistic regression analysis. These factors were further investigated for their impact on tumor visibility in a 3-T MRI.

### 3. Results

#### 3.1. Clinicopathological characteristics

The study included a total of 20 male participants with a mean age of 67.1 years (SD 6.4). They demonstrated a median serum prostate-specific antigen (PSA) level of 5.8 ng/mL (IQR 4.7–10.2). Mean prostate volume was 35.0 mL (SD 9.5). Pathologically, 13 patients were diagnosed with GS 7 (3 + 4), and 7 patients with GS 7 (4 + 3) adenocarcinomas, with a recorded median GP4 percentage at 30% (IQR 10%–60%). The median volume of tumor relative to the prostate, as recorded by the pathologist, was 9% (IQR 6%–24%).

A total of 54 prostate cancers were pathologically confirmed from the 20 patients. Tumor visibility was confirmed in 16 out of 20 patients [0.80, 95% confidence interval (CI) 0.56–0.94], 26 out of 54 lesions (0.48, 95% CI 0.34–0.62) (Fig. 2). Among the 16 patients showing tumor visibility, the concordance rate between the index tumor set by the radiologist and pathologist was 0.88 (95% CI 0.62–0.98).

#### 3.2. Exploration of variables associated with tumor visibility

The GP4 percentage (48.4% vs. 8.8%,  $P < 0.01$ ) and size (17.4 mm vs. 9.8 mm,  $P = 0.01$ ) of pathologically-determined index tumor were significantly higher in patients with confirmed tumor visibility compared to those without. There were no significant differences in PSA level, prostate volume, the proportion of tumor within the entire prostate, grade, and location of pathologically-determined index tumor (Table 1).

When the analysis was expanded to include all tumors, the GP4 percentage (44.4% vs. 12.0%,  $P < 0.01$ ) and size (10.5 mm vs. 5.3 mm,  $P < 0.01$ ) of visible tumors were still significantly higher than those of invisible tumors. Lesions located in non-apical locations were more prevalent in visible tumors ( $P = 0.04$ ). However, there was no significant difference in the zonal location of lesions between visible and invisible tumors (Table 3).

In the univariable logistic regression analysis, GP4 percentage, pathologically measured tumor size, and the non-apical location of the lesion were selected for the multivariable analysis. The results of the multivariable analysis revealed that GP4 percentage [odds ratio (OR) 1.09] and tumor size (OR 1.36) were factors associated with tumor visibility. The presence of the lesion in the peripheral zone (PZ) location did not show significant association with tumor visibility ( $P = 0.87$ ). The results of the logistic regression analysis have been summarized in Table 2.

When measuring the area under the ROC curves with tumor visibility as the classification variable, both GP4 percentage and tumor size was recorded as 0.88. The value was significantly higher compared to area 0.50, with no evident superiority between the two variables (Fig. 3).

#### 3.3. Literature search for associated variables

In light of the findings, that GP4 percentage and pathological size influence tumor visibility on the 7-T *ex-vivo* MRI, we attempted a Medical Literature Analysis and Retrieval System Online (MEDLINE) library search using the following query: (((prostate cancer) OR (prostate neoplasms)) AND ((MRI) OR (magnetic resonance imaging))) AND ((gleason pattern 4) OR (size))) AND (visib\*). The searchtargeted consequently found 65 articles and their references.

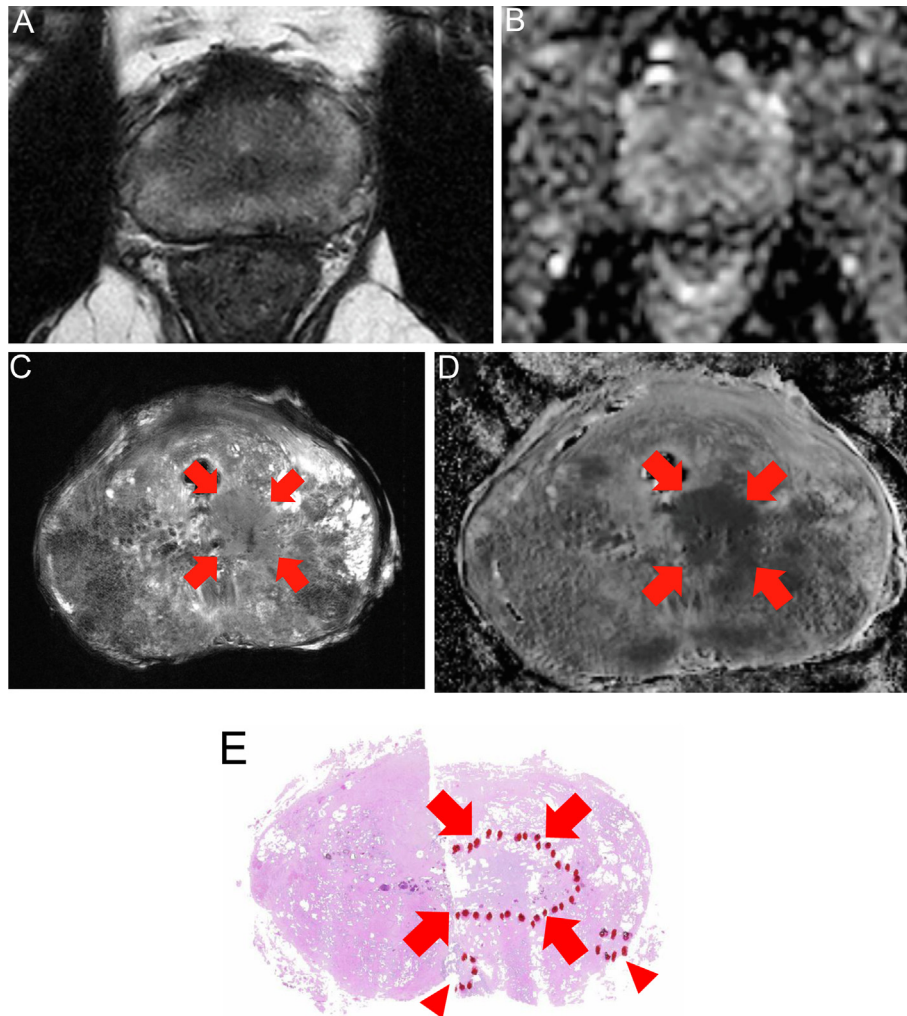


**Fig. 2.** A 60-year-old male with a PSA level of 5.6 ng/mL. Despite the absence of suspicious intra-prostatic lesions on both the T2WI (A) and apparent diffusion coefficient (ADC) map (B) from the pre-operative 3-T MRI, a biopsy identified GS 7 (4 + 3) cancer in the left mid-prostate core. In contrast, *ex-vivo* 7-T MRI T2WI (C) depicted a suspicious lesion in the left mid-prostate transition zone with an unclear margin, disrupting the ducto-glandular texture (arrows). Restricted diffusion was evident on the ADC map (D). Radiologists measured the lesion at 11 mm, assigning a PIRADS 4 score. Whole-mount pathology (E) revealed GS 7 (4 + 3) cancer, occupying 7% of the total gland, along with smaller lesions nearby that were missed on *ex-vivo* MRI. The pathologist measured the tumor at 14 mm. PSA = prostate-specific antigen, T2WI = T2-weighted imaging, ADC = apparent diffusion coefficient, GS = Gleason score, PIRADS = prostate imaging-reporting, and data system.

**Table 1**

Comparison of characteristics between patients with visible and invisible tumors on *ex-vivo* 7-T MRI

	Patients with visible lesions ( <i>n</i> = 16)	Patients without visible lesions ( <i>n</i> = 4)	<i>P</i> value
PSA (ng/mL, median (IQR))	5.61 (4.69–10.2)	7.22 (4.83–13.2)	0.75
Index tumor location			0.79
TZ ( <i>n</i> , %)	13 (81.2)	3 (75.0)	
PZ ( <i>n</i> , %)	3 (18.8)	1 (25.0)	
GP4 proportion of index tumor (%; mean ± SD)	48.4 ± 26.4	8.8 ± 2.5	<0.01
Index tumor grade			0.11
GS 7 (4 + 3) ( <i>n</i> , %)	7 (43.8)	0 (0)	
GS 7 (3 + 4) ( <i>n</i> , %)	9 (56.2)	4 (100)	
Tumor/prostate volume (%; median (IQR))	10 (6–24)	7 (5–24)	0.51
Prostate volume (mL; mean ± SD)	34.9 ± 8.2	35.3 ± 15.6	0.95
Index tumor size on pathology (mm; mean ± SD)	17.4 ± 5.1	9.8 ± 3.0	0.01

PSA, prostate-specific antigen; IQR, inter-quartile range; PZ, peripheral zone; TZ, transition zone; GP4, Gleason pattern 4; SD, standard deviation; GS, Gleason score.

Ten studies provided profiles for tumor grade and size, and the results are summarized in Table 4.<sup>12–21</sup> In 3-T MRI, invisible tumors showed GP4 percentage ranging from 15% to over 30%. More than half of the available studies suggested GS 7 (4 + 3) or more,

i.e. GP4 percentage > 50%, as a threshold where visible tumors outnumbered invisible tumors. The sizes of 3-T MRI-invisible tumors ranged from 0.7 cm to 1.7 cm, all larger than in our study (5.3 mm).

**Table 2**  
Comparison of characteristics between visible and invisible tumors on ex-vivo 7-T MRI

	Visible tumors (n = 26)	Invisible tumors (n = 28)	P value
Tumor location			0.87
PZ (n, %)	20 (76.9)	21 (75.0)	
TZ (n, %)	6 (23.1)	7 (25.0)	
GP4 percentage (% median (IQR))	44.4 (20–60)	12.0 (0–20)	<0.01
Tumor grade			<0.01
GS 7 (4 + 3) (n, %)	11 (42.3)	0 (0)	
GS 7 (3 + 4) (n, %)	15 (57.7)	20 (71.4)	
GS 6 (3 + 3) (n, %)	0 (0)	8 (28.6)	
Tumor level			0.04
Apical (n, %)	2 (7.7)	8 (28.6)	
Nonapical (n, %)	24 (92.3)	20 (71.4)	
Tumor size on pathology (mm, mean ± SD)	10.5 ± 4.0	5.3 ± 2.1	<0.01

PZ, peripheral zone; TZ, transition zone; GP4, Gleason pattern 4; IQR, inter-quartile range; GS, Gleason score; SD, standard deviation.

**Table 3**  
Factors influencing tumor visibility on ex-vivo 7-T MRI: univariable and multivariable logistic regression analyses

Variables	Univariable		Multivariable	
	Odds ratio (95% CI)	P value	Odds ratio (95% CI)	P value
Proportion of GP4	1.11 (1.04–1.17)	<0.01	1.09 (1.01–1.18)	0.02
Size on pathology	1.54 (1.23–1.93)	<0.01	1.36 (1.04–1.79)	0.03
Non-apical level	3.90 (0.97–15.6)	0.06	2.41 (0.43–13.7)	0.32
PZ location	0.90 (0.26–3.14)	0.87	N/A	

CI, confidence interval; GP4, Gleason pattern 4; PZ, peripheral zone; N/A, not applicable.

3.4. Comparison of tumor size between MRI and pathology

For the 26 lesions categorized as PIRADS score 4 or 5 on MRI, the radiologists measured them with an average size of 7.7 mm (SD 3.1), whereas the pathologist recorded an average size of 10.5 mm (SD 4.1). Consequently, pathology tended to assess the size of PCa as larger. The mean difference of 2.7 mm (SD 3.2) was statistically

significant ( $P < 0.01$ ). Fig. 4 illustrates the Bland–Altman plot for these lesions.

4. Discussion

Previous studies in the realm of ex-vivo UHF MRI have focused on refining near-microscopic resolution<sup>10</sup>, and comparing histology with functional sequences<sup>22,23</sup>. The only ex-vivo UHF bpMRI study we discovered attempted to evaluate the surgical margins of specimens<sup>24</sup>. Prior research on the tumor detection capabilities of ex-vivo UHF bpMRI is thus limited. Furthermore, existing studies in this domain have employed small sample sizes, typically fewer than 15 study subjects, primarily because of their experimental nature.

Our study focused on patients diagnosed with csPCa through biopsy, despite not having visible lesions on preoperative in-vivo 3-T MRI. The invisibility of the csPCa on MRI prevents the omission of systematic biopsies in the diagnosis of prostate cancer, potentially leading to an increase in the number of biopsy cores and the likelihood of complications. Moreover, the presence of csPCa is not visible on the MRI could contribute to uncertainty in the management of patients undergoing an active surveillance. The fact that majority of patients included in our study demonstrated tumor visibility on the ex-vivo MRI suggests the potential for 7-T MRI to be a notable innovation in the field of PCa diagnosis in the future.

Our findings thus align with established knowledge regarding the impact of tumor grade and size on visibility in MRI. Cai et al asserted that tumor size, the presence of GP4, and the presence of lesions in the peripheral zone (PZ) were factors influencing tumor visibility<sup>20</sup>. We did verify that our findings were somewhat similar to theirs; tumor size and GP4 percentage were still associated with tumor visibility even on the 7-T ex-vivo MRI. This implies that the detection of clinically insignificant PCa, characterized by low grade or small size, may not significantly increase even with the widespread use of UHF MRI. Moreover, the GP4 percentage of 3-T MRI-invisible tumors, previously reported in past studies to be 15%–34%, was observed to be around 10% in our study, further indicating the superior resolution of 7-T MRI<sup>16,21</sup>.

On the other hand, the zonal location of lesions did not emerge as a factor influencing tumor visibility in our study. Generally, detecting cancer in the transition zone (TZ) using MRI poses a more challenging task compared to the PZ cancer detection. This difficulty arises due to the potential overlap of imaging features between cancer and the prevalent benign prostatic hyperplasia in the TZ<sup>25</sup>. The primary aim of the most recent update to PIRADS v2.1 in 2019 was also focused on improving the interpretation of TZ lesions<sup>26</sup>. Due to the current limitations of MRI, research is also being conducted to explore the use of alternative biomarkers for

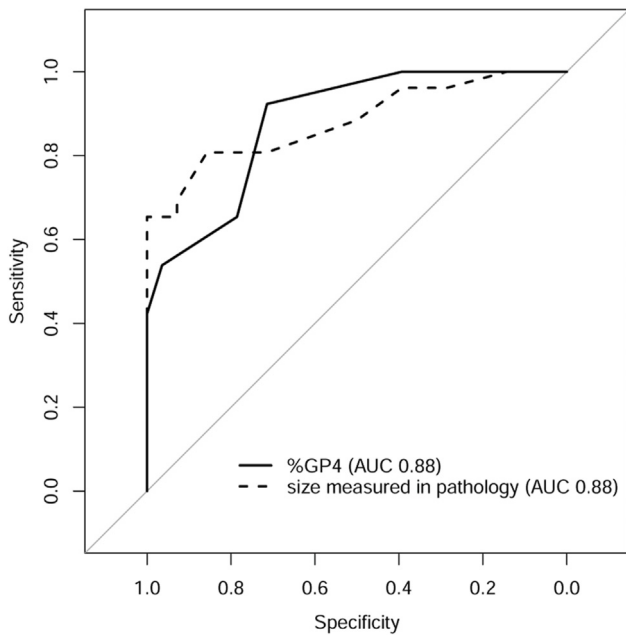


**Fig. 3.** ROC curves for %GP4 and tumor size on pathology, with tumor visibility as a dependent variable. Both explanatory variables demonstrated an identical area under the curve (AUC) of 0.88. ROC = receiver-operating characteristics, %GP4 = Gleason pattern 4 percentage, AUC = area under the curve.

**Table 4**  
Comparison of prior studies investigating grade and size of 3T MRI-invisible prostate cancer

Study	N	Invisible tumor %GP4	Grade threshold (GS)	Invisible tumor size (cm)	Size threshold (cm)	Comment
Turkbey 2011	45	N/A	8 (4 + 4)	N/A	0.5	
Delongchamps 2015	125	0–20	N/A	0.7	N/A	Spherical tumor shape assumed to calculate diameter
Le 2015	122	N/A	7 (3 + 4)	N/A	1.1–2.0	
Truong 2017	22	N/A	7 (3 + 4)	N/A	0.5	
Miyai 2019	59	34	N/A	1.4	N/A	
Park 2019	59	N/A	7 (4 + 3)	1.5	N/A	
Wang 2019	55	N/A	8 (4 + 4)	N/A	1.5–3.0	
Shin 2021	214	N/A	7 (4 + 3)	1.7	N/A	Spherical tumor shape assumed to calculate diameter
Cai 2022	117	0–20	7 (4 + 3)	1.0	N/A	
Chatterjee 2023	61	15	N/A	1.4	N/A	

Grade and size thresholds for MRI-visible tumors surpassing invisible tumors.

N, number of patients included; %GP4, Gleason pattern 4 proportion; GS, Gleason score; N/A, not applicable.

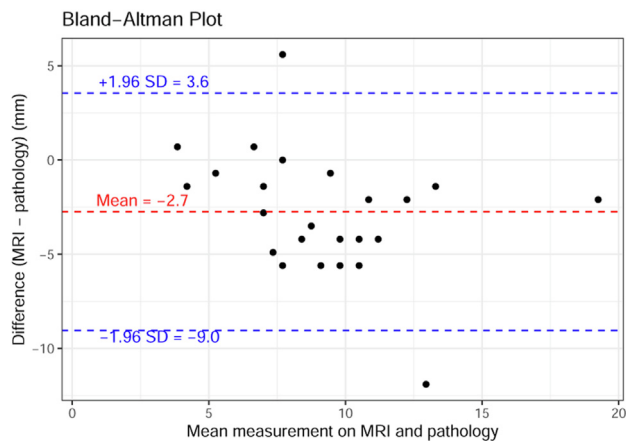


**Fig. 4.** Bland-Altman plot depicting the comparison between tumor size measurements obtained from *ex-vivo* MRI and pathology. Pathology exhibited an average measurement 2.7 mm larger than that of *ex-vivo* MRI for tumor size.

distinguishing benign prostatic hyperplasia and TZ cancer<sup>27</sup>. However, the fact that a significant number of lesions not visible on preoperative 3T MRI have demonstrated visibility on the 7-T *ex-vivo* MRI, while the zonal location did not contribute to visibility, raise expectations that UHF MRI enhance the differentiation between benign prostatic hyperplasia and TZ cancer.

Another noteworthy aspect of our study's results was the size of visible and invisible tumors on MRI. In the aforementioned study by Cai et al, the sizes of MRI-visible and invisible tumors were 13 mm and 10 mm, respectively<sup>20</sup>. In our study, these values were smaller at 10.5 mm and 5.3 mm, respectively, which may be due to the improved resolution of UHF MRI. The commonly accepted volume criterion for defining a csPCa is 0.5 mL<sup>28</sup>. Assuming a spherical shape, a tumor with a diameter of 10.5 mm has a volume of 0.6 mL, while a lesion with a diameter of 5.3 mm is less than 0.1 mL. The volume criteria for csPCa fall in between these values, indicating that the resolution of UHF MRI was adequate. Additionally, the sizes of 3-T MRI-invisible tumors found through literature search ranged from 0.7 cm to 1.7 cm, confirming that they are larger than the 5.3 mm reported in our study<sup>13,16,17,19–21</sup>. This observation also raises the expectation that the higher spatial resolution of 7-T MRI may enable the detection of smaller tumors.

The fact that the difference between the pathological and radiological size of the tumor in our study was smaller compared to the existing evidence was another result raising expectations for improved resolution of 7-T MRI. Pooli et al reported that the tumor

size measured on the MRI is on an average 8 mm smaller than that measured on pathology<sup>5</sup>. In our study, this difference was reduced to 3 mm. Particularly noteworthy is that our study was conducted without DCE MRI, while Sun et al's research suggests that DCE MRI may contribute to providing the tumor size closest to pathology<sup>6</sup>. Therefore, the widespread use of UHF MRI and the implementation of DCE MRI are expected to further contribute to resolving this discrepancy.

We cannot overlook some limitations in our study. Firstly, it is a small-scale study conducted at a single institution, which is an inevitable challenge due to the experimental setting. Overcoming this limitation may be possible in the future when the routine use of UHF MRI beyond 3-T is established. Secondly, since the MRI was performed *ex-vivo*, caution is advised in extrapolating the promising results of this study directly to *in-vivo* MRI. However, considering the presence of factors such as post-biopsy hemorrhage and the absence of DCE MRI, which can adversely affect interpretation in *ex-vivo* imaging, it cannot be definitively asserted that the results of *in-vivo* MRI would be more negative<sup>29,30</sup>.

In conclusion, *ex-vivo* 7-T MRI of RP specimens revealed that the majority of csPCa patients exhibited tumor visibility on UHF MRI, despite negative results from initial 3-T preoperative MRI. The visibility of tumors was found to be influenced by GP4 percentage and size on pathology. The smaller mean size of both MRI-visible and invisible tumors, along with a reduced size discrepancy between MRI and pathology, suggests potential improvements in resolution of UHF MRI.

## Conflict of interest

There is no conflict of interest.

## References

- Bergengren O, Pekala KR, Matsoukas K, Fainberg J, Mungovan SF, Bratt O, et al. 2022 Update on prostate cancer epidemiology and risk factors – a systematic review. *Eur Urol* 2023;84:191–206.
- Ahn H. Prostate biopsy: general consideration and systematic biopsy. *J Korean Soc Radiol* 2023;84:1211–1219.
- Mohammadian Bajgiran A, Afshari Mirak S, Shakeri S, Felker ER, Ponzini D, Ahuja P, et al. Characteristics of missed prostate cancer lesions on 3T multiparametric-MRI in 518 patients: based on PI-RADSv2 and using whole-mount histopathology reference. *Abdom Radiol (NY)* 2019;44:1052–1061.
- Baco E, Rud E, Eri LM, Moen G, Vlatkovic L, Svindland A, et al. A randomized controlled trial to assess and compare the outcomes of two-core prostate biopsy guided by fused magnetic resonance and transrectal ultrasound images and traditional 12-core systematic biopsy. *Eur Urol* 2016;69:149–156.
- Pooli A, Johnson DC, Shirk J, Markovic D, Sadun TY, Sisk Jr AE, et al. Predicting pathological tumor size in prostate cancer based on multiparametric prostate magnetic resonance imaging and preoperative findings. *J Urol* 2021;205:444–451.

6. Sun C, Chatterjee A, Yousuf A, Antic T, Eggener S, Karczmar GS, et al. Comparison of T2-weighted imaging, DWI, and dynamic contrast-enhanced MRI for calculation of prostate cancer index lesion volume: correlation with whole-mount pathology. *Am J Roentgenol* 2019;212:351–356.
7. Steensma BR, Luttje M, Voogt IJ, Klomp DWJ, Luijten PR, van den Berg CAT, et al. Comparing signal-to-noise ratio for prostate imaging at 7T and 3T. *J Magn Reson Imaging* 2019;49:1446–1455.
8. Erturk MA, Tian J, Van de Moortele PF, Adriany G, Metzger GJ. Development and evaluation of a multichannel endorectal RF coil for prostate MRI at 7T in combination with an external surface array. *J Magn Reson Imaging* 2016;43:1279–1287.
9. Tenbergen CJA, Metzger GJ, Scheenen TWJ. Ultra-high-field MR in prostate cancer: feasibility and potential. *Magma* 2022;35:631–644.
10. Durand M, Jain M, Robinson B, Aronowitz E, El Douahy Y, Leung R, et al. Magnetic resonance microscopy may enable distinction between normal histomorphological features and prostate cancer in the resected prostate gland. *BJU Int* 2017;119:414–423.
11. Ranganathan P, Pramesh CS, Aggarwal R. Common pitfalls in statistical analysis: logistic regression. *Perspect Clin Res* 2017;8:148–151.
12. Turkbey B, Mani H, Shah V, Rastinehad AR, Bernardo M, Pohida T, et al. Multiparametric 3T prostate magnetic resonance imaging to detect cancer: histopathological correlation using prostatectomy specimens processed in customized magnetic resonance imaging based molds. *J Urol* 2011;186:1818–1824.
13. Delongchamps NB, Lefevre A, Bouazza N, Beuvon F, Legman P, Cornud F. Detection of significant prostate cancer with magnetic resonance targeted biopsies – should transrectal ultrasound-magnetic resonance imaging fusion guided biopsies alone be a standard of care? *J Urol* 2015;193:1198–1204.
14. Le JD, Tan N, Shkolyar E, Lu DY, Kwan L, Marks LS, et al. Multifocality and prostate cancer detection by multiparametric magnetic resonance imaging: correlation with whole-mount histopathology. *Eur Urol* 2015;67:569–576.
15. Truong M, Hollenberg G, Weinberg E, Messing EM, Miyamoto H, Frye TP. Impact of Gleason subtype on prostate cancer detection using multiparametric magnetic resonance imaging: correlation with final histopathology. *J Urol* 2017;198:316–321.
16. Miyai K, Mikoshi A, Hamabe F, Nakanishi K, Ito K, Tsuda H, et al. Histological differences in cancer cells, stroma, and luminal spaces strongly correlate with in vivo MRI-detectability of prostate cancer. *Mod Pathol* 2019;32:1536–1543.
17. Park KJ, Kim MH, Kim JK, Cho KS. Characterization and PI-RADS version 2 assessment of prostate cancers missed by prebiopsy 3-T multiparametric MRI: correlation with whole-mount thin-section histopathology. *Clin Imaging* 2019;55:174–180.
18. Wang M, Janaki N, Buzzy C, Bukavina L, Mahran A, Mishra K, et al. Whole mount histopathological correlation with prostate MRI in Grade I and II prostatectomy patients. *Int Urol Nephrol* 2019;51:425–434.
19. Shin TJ, Jung W, Ha JY, Kim BH, Kim YH. The significance of the visible tumor on preoperative magnetic resonance imaging in localized prostate cancer. *Prostate Int* 2021;9:6–11.
20. Cai Q, Costa DN, Metter CK, Goldberg K, Roehrborn CG, Cadeddu J, et al. Sensitivity of multiparametric MRI and targeted biopsy for detection of adverse pathologies (Cribriform Gleason pattern 4 and intraductal carcinoma): correlation of detected and missed prostate cancer foci with whole mount histopathology. *Urol Oncol* 2022;40:452 e1–e8.
21. Chatterjee A, Gallan A, Fan X, Medved M, Akurati P, Bourne RM, et al. Prostate cancers invisible on multiparametric MRI: pathologic features in correlation with whole-mount prostatectomy. *Cancers* 2023;15.
22. Sahebjavaheer RS, Nir G, Gagnon LO, Ischia J, Jones EC, Chang SD, et al. MR elastography and diffusion-weighted imaging of ex vivo prostate cancer: quantitative comparison to histopathology. *NMR Biomed* 2015;28:89–100.
23. Uribe CF, Jones EC, Chang SD, Goldenberg SL, Reinsberg SA, Kozlowski P. In vivo 3T and ex vivo 7T diffusion tensor imaging of prostate cancer: correlation with histology. *Magn Reson Imaging* 2015;33:577–583.
24. Heidkamp J, Hoogenboom M, Kovacs IE, Veltien A, Maat A, Sedelaar JPM, et al. Ex vivo MRI evaluation of prostate cancer: localization and margin status prediction of prostate cancer in fresh radical prostatectomy specimens. *J Magn Reson Imaging* 2018;47:439–448.
25. Gholizadeh N, Greer PB, Simpson J, Goodwin J, Fu C, Lau P, et al. Diagnosis of transition zone prostate cancer by multiparametric MRI: added value of MR spectroscopic imaging with sLASER volume selection. *J Biomed Sci* 2021;28:54.
26. Wei CG, Zhang YY, Pan P, Chen T, Yu HC, Dai GC, et al. Diagnostic accuracy and interobserver agreement of PI-RADS Version 2 and Version 2.1 for the detection of transition zone prostate cancers. *Am J Roentgenol* 2021;216:1247–1256.
27. Kim SS, Lee SC, Lim B, Shin SH, Kim MY, Kim SY, et al. DNA methylation biomarkers distinguishing early-stage prostate cancer from benign prostatic hyperplasia. *Prostate Int* 2023;11:113–121.
28. Epstein JI, Chan DW, Sokoll LJ, Walsh PC, Cox JL, Rittenhouse H, et al. Non-palpable stage T1c prostate cancer: prediction of insignificant disease using free/total prostate specific antigen levels and needle biopsy findings. *J Urol* 1998;160:2407–2411.
29. Huebner NA, Korn S, Resch I, Grubmuller B, Gross T, Gale R, et al. Visibility of significant prostate cancer on multiparametric magnetic resonance imaging (MRI) – do we still need contrast media? *Eur Radiol* 2021;31:3754–3764.
30. Caglic I, Barrett T. Optimising prostate mpMRI: prepare for success. *Clin Radiol* 2019;74:831–840.